# Accepted Manuscript

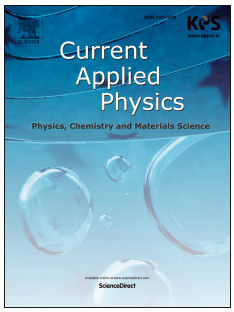


Investigating the magnetic entropy change in single-phase $Y_2Fe_{17}$ melt-spun ribbons

J.L. Sánchez Llamazares, Pablo Álvarez-Alonso, C.F. Sánchez-Valdés, P.J. Ibarra-Gaytán, J.A. Blanco, Pedro Gorria

PII: S1567-1739(16)30126-2

DOI: 10.1016/j.cap.2016.05.013

Reference: CAP 4237

To appear in: *Current Applied Physics*

Received Date: 3 March 2016

Revised Date: 5 May 2016

Accepted Date: 17 May 2016

Please cite this article as: J.L. Sánchez Llamazares, P. Álvarez-Alonso, C.F. Sánchez-Valdés, P.J. Ibarra-Gaytán, J.A. Blanco, P. Gorria, Investigating the magnetic entropy change in single-phase $Y_2Fe_{17}$ melt-spun ribbons, *Current Applied Physics* (2016), doi: 10.1016/j.cap.2016.05.013.

# Investigating the magnetic entropy change in single-phase $Y_2Fe_{17}$ melt-spun ribbons

J. L. Sánchez Llamazares,[1,] Pablo Álvarez-Alonso,[2] C. F. Sánchez-Valdés,[1,3]
P. J. Ibarra-Gaytán,[1] J. A. Blanco,[4] and Pedro Gorria[5,†]

[1]*Instituto Potosino de Investigación Científica y Tecnológica, Camino a la Presa San José 2055 Col. Lomas 4ª, San Luis Potosí, S.L.P. 78216, México.*
[2]*Departamento de Electricidad y Electrónica, Universidad del País Vasco (UPV/EHU), 48940 Leioa, Spain.*
[3]*Centro de Nanociencias y Nanotecnología, Universidad Nacional Autónoma de México, AP 14, Ensenada 22860, Baja California, México.*
[4]*Departamento de Física, Universidad de Oviedo, 33007 Oviedo, Spain.*
[5]*Departamento de Física, EPI, Universidad de Oviedo, 33203 Gijón, Spain.*

† Corresponding author: pgorria@uniovi.es

**Abstract.** The inspection of simplified fabrication and/or processing routes in order to produce materials with attractive magnetocaloric properties is of paramount importance for the development of environmentally friendly magnetic cooling technology. In this work, we have made use of the melt-spinning technique to obtain directly single-phase $Y_2Fe_{17}$ polycrystalline ribbons avoiding any high-temperature annealing for phase consolidation and homogenization. The melt-spun ribbons, with hexagonal $Th_2Ni_{17}$-type crystal structure, exhibit a moderate maximum value of the magnetic entropy change, $|\Delta S_M^{peak}|$ = 2.4(4.4) J kg$^{-1}$ K$^{-1}$ under an applied magnetic field change of 2(5) T. Although these values are similar to those for the bulk alloy, the $\Delta S_M(T)$ curves are manifestly broader, thus giving rise to an expansion of the working temperature range and the enhancement of about 15% in the refrigerant capacity. We also show that the magnetic field dependence of $|\Delta S_M^{peak}|$ at $T = T_C$ follows a $H^{2/3}$ power-law.

***Keywords***: $Y_2Fe_{17}$ intermetallics; melt-spun ribbons; magnetocaloric effect; magnetic entropy change; refrigerant capacity.

## 1. INTRODUCTION

An important challenge of modern society consists in reducing energy consumption through the development of more energy efficient technologies of massive use [1]. Consequently, national and international funding agencies are promoting research and development focused on this target. Commercial refrigeration is a typical example in which the search for a more proficient and clean technology is needed [2]. Therefore, magnetic refrigeration, a solid-state technology based in the magnetocaloric (MC) effect, attracts great interest because it is considered a feasible alternative for the conventional air-compressed refrigerant systems due to, among other advantages, its higher efficiency (of up to 60 % of Carnot's cycle) [3-5]. One of the most active fronts in the field is the development of MC materials with enhanced refrigerant properties [2,6].

Materials with second-order magnetic phase transition (SOMPT) exhibit appealing characteristics for magnetic refrigeration such as the absence of thermal hysteresis and the smoothness of the transition [7-9]. Moreover, SOMPT materials provide a broader temperature interval for the MC effect thus favouring remarkable values of the refrigerant capacity (*RC*), a magnitude which permits an estimation of how much heat can be absorbed at the cold end of the thermodynamic cycle and expelled through the hot end [10]. Amongst these SOMPT materials, Fe-rich $R_2Fe_{17}$ binary intermetallic compounds with R = Y, Pr or Nd are certainly interesting due to a combination of rather high saturation magnetization and near room temperature Curie point ($T_C$ = 303, 335, and 285 K, respectively), together with a low amount of rare-earth content [11,12]. Recent works on the MC behaviour of these Fe-rich alloys in bulk form confirm the moderate values for the maximum magnetic entropy change, $|\Delta S_M^{peak}| \approx 6$ J kg$^{-1}$ K$^{-1}$ and refrigerant capacity $RC \approx 500$ J kg$^{-1}$ under a magnetic field change $\mu_o \Delta H = 5$ T [11-14].

Cooling (or heating) devices based on magnetic refrigeration technology require fast heat exchange in the cold and hot ends of the thermodynamic cycle between the MC material and the fluid heat exchanger [2]; MC materials with large surface to volume ratios, and more precisely melt-spun ribbons, can satisfy such condition [15]. Moreover, the melt-spinning method is a one-

step and low-cost fabrication process for $R_2Fe_{17}$ ribbons, which avoids the high-temperature long-time processing needed for the phase homogenization in conventional bulk alloys. In addition, the integration of melt-spun $Y_2Fe_{17}$ ribbons into heat exchangers for magnetic refrigerators and the magnetocaloric performance of parallel-staked ribbons with micro- and nanocrystalline microstructure is currently being considered [16]. However, the MC effect in melt-spun $R_2Fe_{17}$ ribbons remains almost unexplored except for the pseudo-binary $NdPrFe_{17}$ alloy [17], and a preliminary study performed under a low applied magnetic field (i.e., 1 T) on $Y_2Fe_{17}$ [18].

The aim of this work is to provide a detailed investigation on the magnetic and magnetocaloric properties of single-phase $Y_2Fe_{17}$ melt-spun ribbons. Our results are compared with those obtained for a synthesized bulk alloy and also with data reported in the preliminary study carried out by Fang et al. [18].

## 2. EXPERIMENTAL PROCEDURE.

Polycrystalline ribbons with nominal composition $Y_2Fe_{17}$ were produced by rapid solidification using a homemade melt spinning set-up at a linear speed of the copper wheel of 20 $ms^{-1}$ from bulk pellets previously obtained by arc melting. Pure metallic elements were used as raw materials ($\geq$ 99.9 %). Both the arc-melted starting alloys and the melt-spun ribbons were fabricated under a highly pure Ar atmosphere. For comparison purposes, one of these arc-melted pellets was annealed at 1373 K in a vacuumed quartz ampoule for 1 week; after annealing the sample was quenched in water.

The microstructure and elemental composition of the ribbons were analysed in different ribbon pieces using a FEI Dual beam Helios Nanolab FIB scanning electron microscope (SEM) equipped with an energy dispersive spectroscopy (EDS) system. The resulting composition of the as-cast ribbons coincides with the nominal one within experimental uncertainty. The room temperature X-ray powder diffraction (XRD) pattern was collected in a finely powdered ribbon sample in order to promote a random orientation of the crystallites, thus avoiding texture and/or preferential orientation effects. The experiment was conducted in a Bruker AXS model D8 Advance

X-ray powder diffractometer using Cu-Kα radiation (λ = 1.5418 Å), within the angular range $20^o \leq 2\theta \leq 80^o$ and a step increment of $0.01^o$. The diffraction pattern was analysed using the FullProf suite package based on the Rietveld method [19].

Magnetic measurements were performed using the vibrating sample magnetometer option of a 9 T Quantum Design PPMS® EverCool®-I platform. The magnetic field $\mu_o H$ was applied along the ribbon axis (i.e., the rolling direction) in order to minimize the demagnetizing field effect. The low-field ($\mu_o H$ = 5 mT) magnetization as a function of temperature, $M(T)$, was measured between 200 and 400 K in order to accurately determine the value of the Curie temperature, $T_C$, from the minimum of the $dM/dT$ vs. $T$ curve. Furthermore, a set of isothermal magnetization curves, $M(\mu_o H)$, were collected in the temperature range of 195-400 K with a $\Delta T$ step of 5 K up to a maximum applied magnetic field of 5 T. Then, the $\Delta S_M(T)$ curves were calculated from numerical integration of the Maxwell relation:

$$\Delta S_M(T, \mu_0 H) = \mu_0 \int_0^{\mu_0 H} \left[\frac{\partial M(T', H')}{\partial T'}\right]_{T'=T} dH'$$

For each isothermal $M(\mu_o H)$ curve, the magnetization was measured for a large number of magnetic field values with the aim of minimizing the error in the calculation of $\Delta S_M$. Three different criteria were followed to estimate of the refrigerant capacity, *RC* [8,10,13,20] (a) by finding the product $|\Delta S_M^{peak}| \times \delta T_{FWHM}$ (*RC*-1), where $\delta T_{FWHM} = T_{hot} - T_{cold}$, corresponds to the full-width at half-maximum of the $\Delta S_M(T)$ curve; it is usually assumed that $\delta T_{FWHM}$ coincides with the temperature span of the thermodynamic cycle being $T_{hot}$ and $T_{cold}$ the hot and cold ends, respectively; (b) by calculating the value of the integral area under the $\Delta S_M(T)$ curve between $T_{hot}$ and $T_{cold}$ (*RC*-2); and (c) by maximizing the product $\Delta S_M \times \delta T$ below the $\Delta S_M(T)$ curve (*RC*-3).

## 3. RESULTS AND DISCUSSION

Figure 1 shows four characteristic SEM micrographs of the as-cast $Y_2Fe_{17}$ ribbon. Fig. 1(a) corresponds to a typical cross-sectional view of the ribbons that show an average thickness of 23 ±

2 µm. The microstructure of the ribbons exhibits a disordered polycrystalline growth with grain size values in the range 0.2-2 µm [see Fig. 1(b)], much larger than those found in $NdPrFe_{17}$ ribbons (≈ 10-20 nm) [17]. We can also perceive in the SEM images that both ribbon surfaces are rather smooth and homogeneous on the micrometer length-scale [see Figs. 1(c) and (d) for wheel-side and free-side surfaces, respectively]. Our ribbon samples display a coarse microstructure compared with the previously reported [18]. These differences may be understood taken into account the number of parameters affecting the macroscopic features of the ribbons derived from the melt spinning technique, such as the wheel speed, the temperature of the molten alloys at ejection (which determines its viscosity), the nozzle diameter of the quartz crucible, the distance between the nozzle and the wheel surface or the ejecting over-pressure.

The experimental and calculated X-ray powder diffraction patterns corresponding to the powdered ribbon are depicted in Fig. 2. As a first attempt to properly fit the whole pattern, the two stable crystallographic phases for the $R_2Fe_{17}$ series of compounds were included, namely, the hexagonal $Th_2Ni_{17}$-type (space group $P6_3/mmc$) and the rhombohedral $Th_2Zn_{17}$-type (space group $R\bar{3}m$). However, the best fit clearly indicates that the $Y_2Fe_{17}$ ribbons are single-phase alloys with hexagonal crystal structure, and lattice parameter values $a$ = 8.4602(5) Å and $c$ = 8.3103(6) Å. This result confirms that the formation of a polycrystalline single-phase alloy is straightforward by using the rapid quenching technique, in contrast to conventional arc-melted bulk alloys that usually solidify as a mixture of both rhombohedral and hexagonal phases, and then, additional long time processing at high-temperatures is needed for obtaining a single-phase intermetallic compound. The XRD analysis for the annealed bulk alloy confirmed the formation of a mixture of the hexagonal and rhombohedral phases (in the approximate proportion 75:25); such a mixture has been also observed by other authors in $Y_2Fe_{17}$ bulk alloys synthesized by arc melting and subsequent thermal annealing [21,22].

We can observe from the temperature dependence of the magnetization under a low value of the applied magnetic field [see Fig. 3(a)] for both the $Y_2Fe_{17}$ ribbon and bulk alloys that the two

samples have almost the same Curie temperature, [$T_C$ = 301 ± 1 K and 303 ± 1 for the ribbon and bulk samples, respectively, see inset in Fig. 3(a) for the d$M$/d$T$ vs. $T$ curve], in excellent agreement with previously reported values [12].

In Fig. 3(b) we show the virgin $M(\mu_o H)$ curves for both $Y_2Fe_{17}$ ribbon and bulk samples measured at $T$ = 5 K. The two curves show a similar shape (the slight differences in the low magnetic field range could be ascribed to the different magnetic shape anisotropies expected from the unlike geometries of the specimens), and exhibit a close-to-saturation state under an applied magnetic field above 4 T. The saturation magnetization, $M_S$, has been estimated from a fit of the high-magnetic-field region of the $M(\mu_o H)$ curve to an approach-to-saturation law [23]. The same value, $M_S$ = 144 ± 5 A m$^2$ kg$^{-1}$, is obtained for both samples, being slightly lower than that of the ferromagnetic $Pr_2Fe_{17}$ (162 A m$^2$ kg$^{-1}$) compound [24]. Taking into account that a similar value for the magnetic moment of the Fe atoms in both alloys can be assumed, the non-magnetic character of the yttrium atoms is the responsible for the smaller $M_S$.

The isothermal magnetization curves, $M(\mu_o H)$, for the $Y_2Fe_{17}$ ribbon and the corresponding Arrott plots are given in Figs. 4(a) and 4(b) respectively. The absence of any change in the concavity of any Arrott plot at each single temperature [see Fig. 4(b)], together with the opposed concavity between plots at different temperatures below and above $T_C$, indicates the second order nature of the magnetic phase transition, according to the Banerjee criteria [25]. A first look at the $M(\mu_o H)$ curves shown in Fig. 4(a) reveals that the magnetization is not fully saturated even for $\mu_o H$ = 5 T. This non-saturating behaviour of the $M(\mu_o H)$ curves, which is more evident in the immediacy of $T_C$, is typical of Fe-rich compounds exhibiting strong magneto-volume coupling such as FeNi Invar alloys [26-28]. We have recently reported a similar behaviour in other $R_2Fe_{17}$ alloys (R = Pr, Er or Dy) accompanied by non-vanishing values of the spontaneous magnetostriction in the vicinity of $T_C$. This behaviour is usually originated from short-range magnetic correlations that in $R_2Fe_{17}$ compounds are found to persist up to temperatures as high as $T \approx 1.4\ T_C$ [24,29,30].

Figure 5(a) shows the $|\Delta S_M(T)|$ curves for $Y_2Fe_{17}$ ribbon calculated for selected values of the magnetic field change ranging from 1 to 5 T. The care-like shape of these curves together with the linear trend of $|\Delta S_M^{peak}|$ vs. $(\mu_o \Delta H)^{2/3}$ [see inset of Fig. 5(a)] are typical features of MC materials exhibiting a SOMPT [31]. Figure 5(b) compares the $|\Delta S_M(T)|$ curves (that were obtained under magnetic field changes $\mu_o \Delta H$ = 2 and 5 T) for the as-quenched ribbon and the bulk alloy (see inset for the normalized $\Delta S_M/\Delta S_M^{peak}$ vs. $T/T_C$). In Table I, we present a summary of the data for the MC properties of both materials. In addition, we include also the data reported by Fang et al. [17] under a magnetic field change of 1 T for melt spun ribbons solidified at the wheel speed of 20 $ms^{-1}$. If they are compared with the latter, for $\mu_o \Delta H$ = 1 T *RC*-1 and $\delta T_{FWHM}$ of the fabricated ribbons are superior in 38 % and 75 %, respectively. In addition, there are two remarkable issues in Fig. 5 that deserve a special consideration. Firstly, although the value for $|\Delta S_M^{peak}|$ is almost equal in both samples (but slightly lower than the reported in Ref. [12] under an applied magnetic field change of 5 T for a bulk sample: $|\Delta S_M^{peak}|$ = 5.1 J $kg^{-1}$ $K^{-1}$), the ribbon exhibits an enhancement of the refrigerant capacity that reaches 15 % (see Table I) due to a broadening of the $|\Delta S_M(T)|$ curve for $T > T_C$. Secondly, the ribbon sample displays a $|\Delta S_M(T)|$ curve with a flattening, which is a desirable feature when the Ericsson-like magnetic refrigeration cycle is preferred [10]. The (operating) temperature range where the $|\Delta S_M(T)|$ curve is almost flat reaches $\Delta T \approx 21$ K for $\mu_o \Delta H$ = 5 T, giving rise to an effective refrigerant capacity $RC_{eff} = \Delta T \times |\Delta S_M^{peak}| > 90$ J $kg^{-1}$, larger than that estimated for composite materials made of two or more Fe-based ribbons [32,33].

Figure 6 shows how the values of the refrigerant capacities *RC*-1, *RC*-2, *RC*-3 vary as $\mu_o \Delta H$ is increased up to 5 T. In the inset the evolution of the characteristic temperatures $T_{cold}$ and $T_{hot}$ is plotted as well. The values for these magnitudes are always larger than those for the bulk alloy (see Table I), and for $\mu_o \Delta H$ = 5 T the refrigerant capacity of $Y_2Fe_{17}$ ribbons is roughly 80 % of that reported for Gd (*RC*-1 = 687 J $kg^{-1}$, *RC*-2 = 430 J $kg^{-1}$, *RC*-3 = 283 J $kg^{-1}$) [13]. In fact, this is a consequence of the width of the $\Delta S_M(T)$ curves, $\delta T_{FWHM}^{ribbon}$, which reaches 121 K at $\mu_o \Delta H$ = 5 T,

thus suggesting that the rapid solidification procedure favours the temperature span of the magnetocaloric effect in diverse polycrystalline intermetallic compounds [16,34,35].

## 4. SUMMARY AND CONCLUSIONS

$Y_2Fe_{17}$ has been synthesized in thin ribbon shape by rapid solidification using the melt spinning technique. The polycrystalline ribbons are single-phase alloys with a hexagonal $Th_2Ni_{17}$-type crystal structure. The ribbons exhibit a similar magnetic behaviour to that of the synthesized polycrystalline bulk alloys, with a Curie temperature $T_C \approx 301\pm1$ K and a low temperature saturation magnetization $M_S \approx 144 \pm 5$ A $m^2$ $kg^{-1}$. A moderate magnetocaloric effect is observed around room temperature with an improved refrigerant capacity, roughly 15% superior, compared with that exhibited by the bulk alloy. The one-step process employed largely simplifies the fabrication procedure since it eludes the long-term high-temperature thermal annealing needed to ensure a single-phase when arc-melted bulk $R_2Fe_{17}$ alloys are produced.

## ACKNOWLEDGEMENTS

This work was supported by: (a) projects CB-2010-01-156932 (CONACyT); MAT2014-56116-C4-R (MINECO) and FC-15-GRUPIN14-037 (FICyT); and (b) Laboratorio Nacional de Investigaciones en Nanociencias y Nanotecnología (LINAN, IPICyT). The technical support of Dr. G.J. Labrada-Delgado and B.A. Rivera-Escoto is gratefully acknowledged. C.F. Sánchez-Valdés thanks CTIC-UNAM for supporting his postdoctoral position at CNyN-UNAM; P. Alvarez-Alonso thanks Gobierno Vasco (IT711-13) for supporting his postdoctoral stay; P.J. Ibarra-Gaytán wishes to thank CONACyT for supporting his Ph.D. studies.

## REFERENCES

[1] O. Gutfleisch, M. A. Willard, E. Brück, C.H. Chen, S.G. Sankar, and J. Ping Liu, Adv. Mater. 23 (2011) 821.

[2] A. Kitanovski, J. Tušek, U. Tomc, U. Plaznik, M. Ožbolt, A. Poredoš, *Magnetocaloric Energy Conversion: From Theory to Applications*, (Springer, 2015).

[3] R. Bjørk, C.R.H. Bahl, A. Smith, N. Pryds, Int. J. Refrig. 33 (2010) 437.

[4] B. Yu, M. Liu, P.W. Egolf, A. Kitanovski, Int. J. Refrig. 33 (2010) 1029.

[5] V. Franco, J.S. Blázquez, B. Ingale, A. Conde, Annu. Rev. Mater. Res. 42 (2012) 305.

[6] M.-H. Phan, S.-C. Yu, J. Magn. Magn. Mater. 308 (2007) 325.

[7] K.A. Gschneidner Jr., V.K. Pecharsky, A. O. Tsokol, Rep. Prog. Phys. 68 (2005) 1479.

[8] A.M. Tishin, Y.I. Spichkin, The Magnetocaloric Effect and Its Applications, IOP, Bristol, 2003.

[9] Z. Wang, Q. Xu, K. Chen, Current Appl. Phys. 12 (2012) 1153.

[10] M.E. Wood, W.H. Potter, Cryogenics 25 (1985) 667.

[11] S. Yu. Dan'kov, V.V. Ivtchenko, A.M. Tishin, K.A. Gschneidner, Jr., V.K. Pecharsky, Adv. Cryog. Eng. 46 (2000) 397.

[12] K. Mandal, A. Yan, P. Kerschl, A. Handstein, O. Gutfleisch, K.-H. Muller, J. Phys. D: Appl. Phys. 37 (2004) 2628.

[13] P. Gorria, J.L. Sánchez Llamazares, P. Álvarez, M.J. Pérez, J. Sánchez Marcos, J.A. Blanco, J. Phys. D: Appl. Phys. 41 (2008) 192003.

[14] P. Álvarez, P. Gorria, V. Franco, J.S. Marcos, M.J. Pérez, J.L. Sánchez Llamazares, I. Puente-Orench, J.A. Blanco, J. Phys.: Condens. Mater. 22 (2010) 216005.

[15] V.V. Khovaylo, V.V. Rodionova, S.N. Shevyrtalov, V. Novosad, Phys. Stat. Sol. (b). 251 (2014) 2104.

[16] D. Yu Karpenkov, K.P. Skokov, J. Liu, A. Yu Karpenkov, E.M. Semenova, E.L. Airiyan, Yu G. Pastushenkov, O. Gutfleisch, J. Alloys. Compd. 668 (2016) 40.

[17] C.F. Sánchez-Valdés, P.J. Ibarra-Gaytán, J.L. Sanchez Llamazares, M. Ávalos-Borja, P. Álvarez-Alonso, P. Gorria, J.A. Blanco, Appl. Phys. Lett. 104 (2014) 212401.

[18] Y.K. Fang, C.W. Chang, C.C. Yeh, H.W. Chang, W. Li, W.C. Chang, J. Appl. Phys. 103 (2008) 07B302.

[19] J. Rodríguez-Carvajal, Physica B 192 (1993) 55.

[20] K.A. Gschneidner Jr., V.K. Pecharsky, A.O. Pecharsky, C.B. Zimm, Mater. Sci. Forum 315-317 (1999) 69.

[21] H. Takano, N. Oba, S. Murayama, K. Hoshi, J. Magn. Magn. Mater. 177-181 (1998) 1445.

[22] N.X. Shen, Y.D. Zhang, J.I. Budnick, W.A. Hines, R. Lyver, K.H.J. Buschow, Appl. Phys. Lett. 69 (1996) 3194.

[23] B.D. Cullity, C.D. Graham, Introduction to Magnetic Materials, John Wiley & Sons, New Jersey, 2009.

[24] P. Gorria, P. Álvarez, J.S. Marcos, J.L. Sánchez Llamazares, M.J. Pérez, J.A. Blanco, Acta Mater. 57 (2009) 1724.

[25] B.K. Banerjee, Phys. Lett. 12 (1964) 16.

[26] E.F. Wassermann, J. Magn. Magn. Mater. 100 (1991) 346.

[27] W. Pepperhoff, M. Acet, Constitution and Magnetism of Iron and its Alloys, Springer, Berlin, 2001.

[28] P. Gorria et al., Phys. Rev. B 80 (2009) 064421.

[29] P. Alvarez-Alonso, P. Gorria, J.A. Blanco, J. Sanchez-Marcos, G.J. Cuello, I. Puente-Orench, J.A. Rodriguez-Velamazan, G. Garbarino, I. de Pedro, J. Rodriguez Fernandez, J.L. Sánchez Llamazares, Phys. Rev. B 86 (2012) 184411.

[30] P. Alvarez-Alonso, P. Gorria, J.L. Sánchez Llamazares, G.J. Cuello, I. Puente-Orench, J. Sanchez-Marcos, G. Garbarino, M. Reiffers, J.A. Blanco, Acta Mater. 61 (2013) 7931.

[31] H. Oesterreicher, F.T. Parker, J. Appl. Phys. 55 (1984) 4334.

[32] P. Álvarez, J.L. Sanchez Llamazares, P. Gorria, J.A. Blanco, Appl. Phys. Lett. 99 (2011) 232501.

[33] P. Álvarez, P. Gorria, J.L. Sanchez Llamazares, J.A. Blanco, J. Alloys. Compd. 568 (2013) 98.

[34] P.J. Ibarra-Gaytán, C.F. Sánchez-Valdés, J.L. Sanchez Llamazares, P. Álvarez-Alonso, P. Gorria, J.A. Blanco, Appl. Phys. Lett. 103 (2013) 152401.

[35] J.L. Sanchez Llamazares, C.F. Sánchez-Valdés, P.J. Ibarra-Gaytán, P. Álvarez-Alonso, P. Gorria, J.A. Blanco, J. Appl. Phys. 113 (2013) 17A912.

**TABLE I.** $|\Delta S_M^{peak}|$, *RC*-1, *RC*-2, $\delta T_{FWHM}$, $T_{hot}$, $T_{cold}$, *RC*-3, $\delta T^{RC-3}$, and $T_{hot}^{RC-3}$ and $T_{cold}^{RC-3}$ (i.e., related to *RC*-3) for $Y_2Fe_{17}$ melt-spun ribbons and bulk alloy. All of them are given for magnetic field changes $\mu_o\Delta H$ of 1, 2 and 5 T. The data for $Y_2Fe_{17}$ melt-spun ribbons at $\mu_o\Delta H$ = 1 T was estimated from the magnetic entropy change curve reported in Ref. [18] for the sample solidified at 20 $ms^{-1}$.

| | **Ribbons** | | | **Ribbons** [17] | **Bulk** | |
|---|---|---|---|---|---|---|
| $T_C$ **(K)** | 301 | | | 304 | 303 | |
| $\mu_o\Delta H$ **(T)** | 1 | **2** | **5** | 1 | **2** | **5** |
| $\|\Delta S_M^{peak}\|$ **(J kg$^{-1}$ K$^{-1}$)** | 1.5 | 2.4 | 4.4 | 1.8 | 2.4 | 4.6 |
| ***RC*-1 (J kg$^{-1}$)** | 75 | 178 | 533 | 54 | 156 | 478 |
| ***RC*-2 (J kg$^{-1}$)** | 58 | 138 | 414 | 44 | 121 | 367 |
| $\delta T_{FWHM}$ **(K)** | 51 | 74 | 121 | 29 | 65 | 103 |
| $T_{hot}$ **(K)** | 335 | 351 | 385 | 324 | 339 | 365 |
| $T_{cold}$ **(K)** | 284 | 277 | 264 | 295 | 274 | 262 |
| ***RC*-3 (J kg$^{-1}$)** | 38 | 90 | 270 | - | 82 | 249 |
| $\delta T^{RC-3}$ **(K)** | 62 | 101 | 134 | - | 101 | 126 |
| $T_{hot}^{RC-3}$ **(K)** | 340 | 363 | 391 | - | 353 | 374 |
| $T_{cold}^{RC-3}$ **(K)** | 278 | 262 | 257 | - | 252 | 248 |

## FIGURE CAPTIONS

**FIG. 1.** SEM micrographs of the typical microstructure of as-solidified $Y_2Fe_{17}$ ribbons: (a) fracture cross-section; (b) higher magnification image of the grains at the ribbon cross-section; (c) ribbon wheel-side surface, and; (d) ribbon free surface.

**FIG. 2.** Room temperature experimental and calculated XRD patterns for as-quenched $Y_2Fe_{17}$ melt-spun ribbons. The difference between both patterns is depicted at the bottom of the figure. The vertical green bars correspond to the positions of the Bragg reflections for the $P6_3/mmc$ hexagonal crystal structure.

**FIG. 3.** (a) $M(T)$ curves measured for $Y_2Fe_{17}$ ribbons and bulk alloys under a low value of the applied magnetic field (5 mT). Inset: $dM/dT$ vs. $T$ curve for melt-spun ribbons and bulk alloys. (b) Magnetization curves measured at $T$ = 5 K.

**FIG. 4.** (a) Isothermal magnetization curves, $M(\mu_o H)$, measured in the 195 - 400 K temperature range for as-quenched $Y_2Fe_{17}$ alloy ribbons. (b) Arrott plots corresponding to the magnetization curves in (a).

**FIG. 5.** (a) $|\Delta S_M(T)|$ curves for $\mu_o \Delta H$ between 1 and 5 T for $Y_2Fe_{17}$ melt-spun ribbons. The almost linear behaviour of $|\Delta S_M^{peak}|$ versus $(\mu_o \Delta H)^{2/3}$ is shown in the inset. (b) Comparison of the $|\Delta S_M(T)|$ curves for the as-quenched ribbon and those corresponding to the polycrystalline bulk alloy for $\mu_o \Delta H$ = 2 and 5 T.

**FIG. 6.** Refrigerant capacities *RC*-1, *RC*-2, and *RC*-3 as a function of $\mu_o \Delta H$. for $Y_2Fe_{17}$ ribbons. Inset: $T_{hot}$ and $T_{cold}$ vs. $\mu_o \Delta H$ (see text for details).

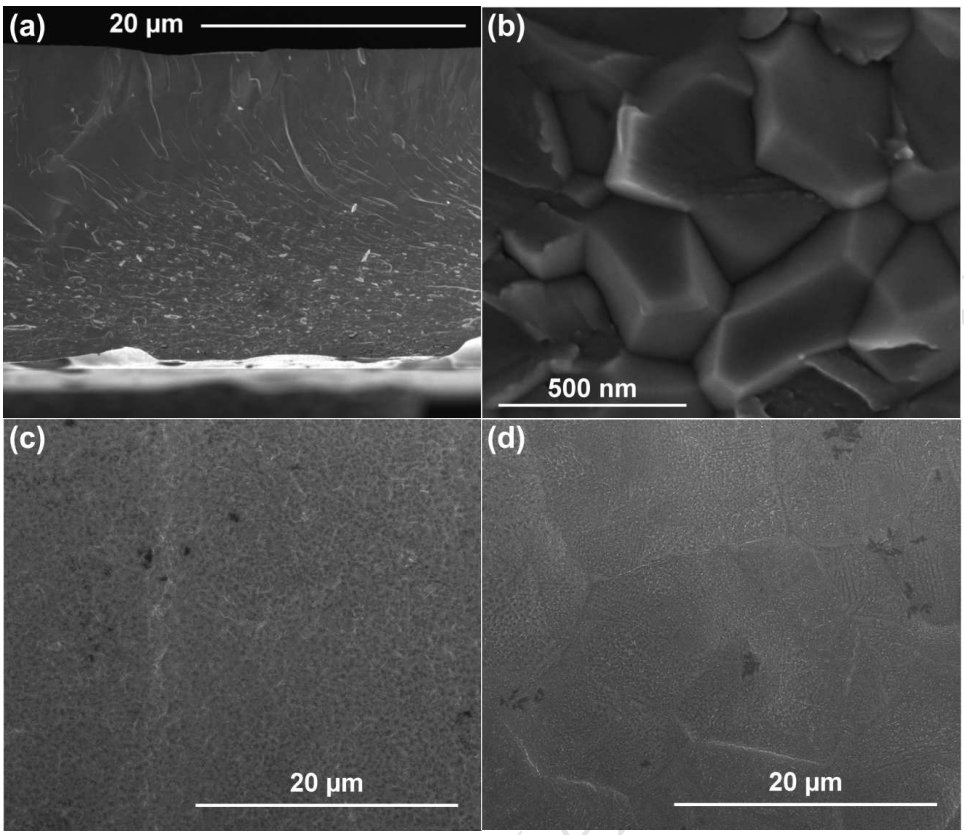


**FIGURE 1**

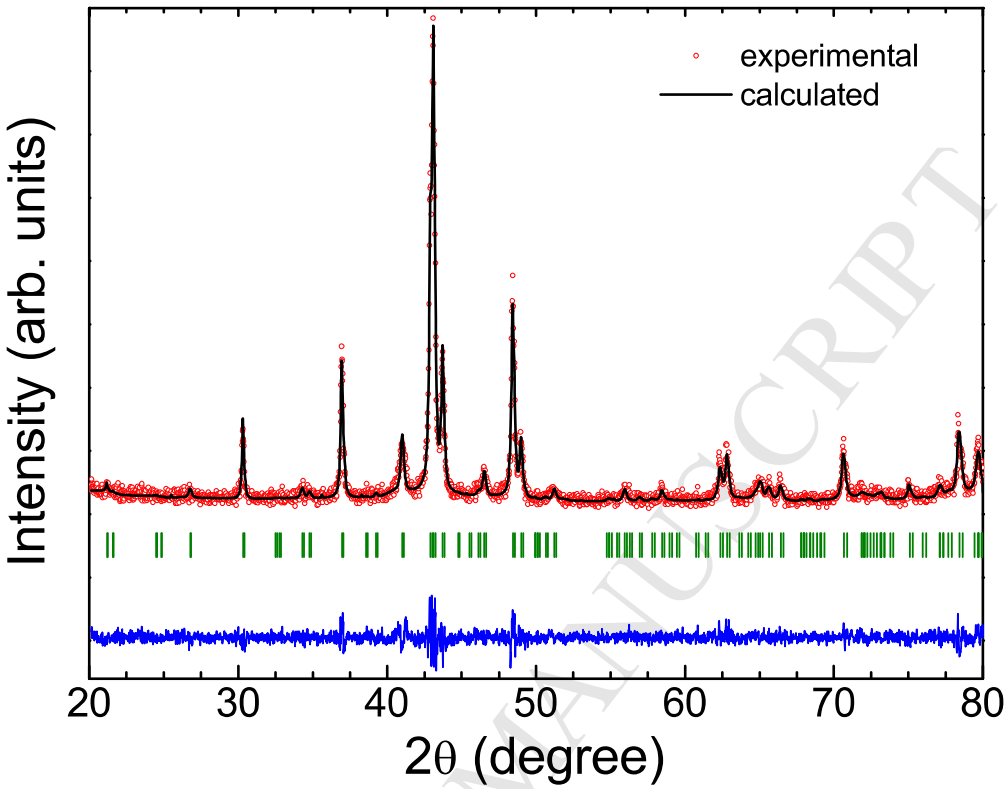


**FIGURE 2**

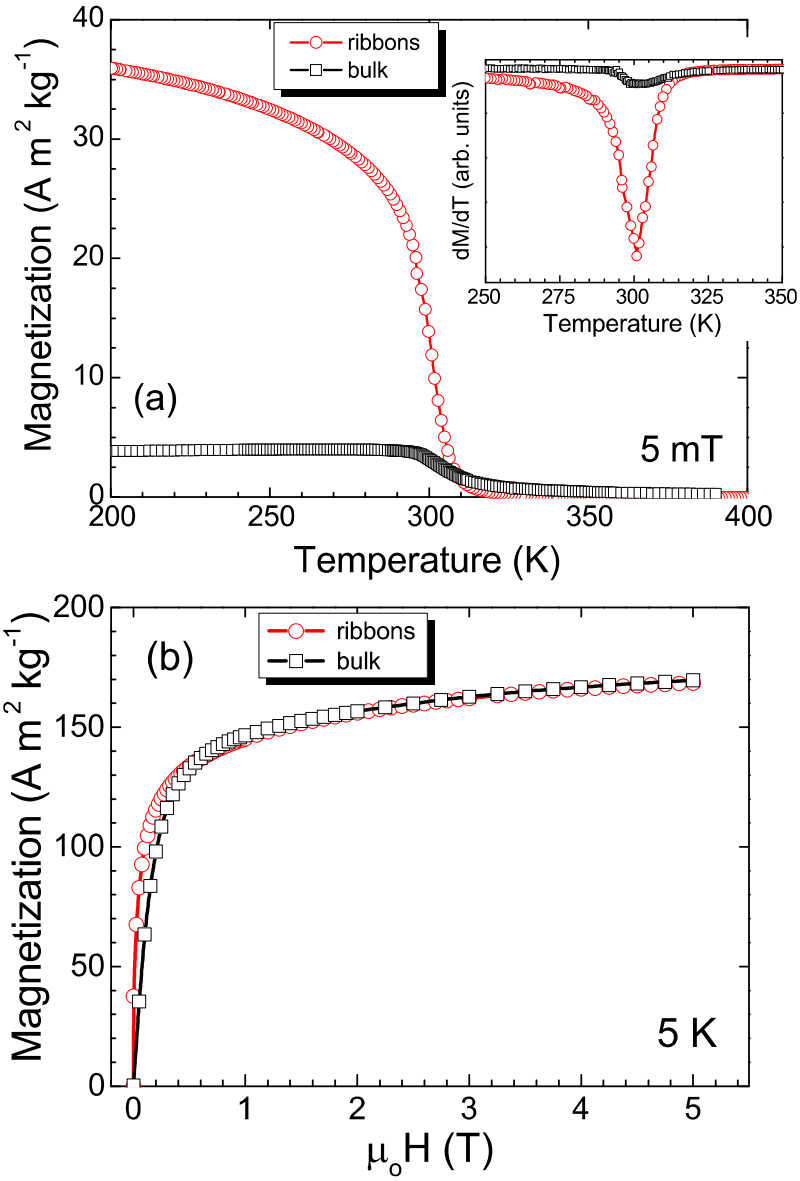
ribbons
bulk
(a)
5 mT
Magnetization (A m$^2$ kg$^{-1}$)
Temperature (K)
dM/dT (arb. units)
Temperature (K)
(b)
5 K
$\mu_o$H (T)

FIGURE 5

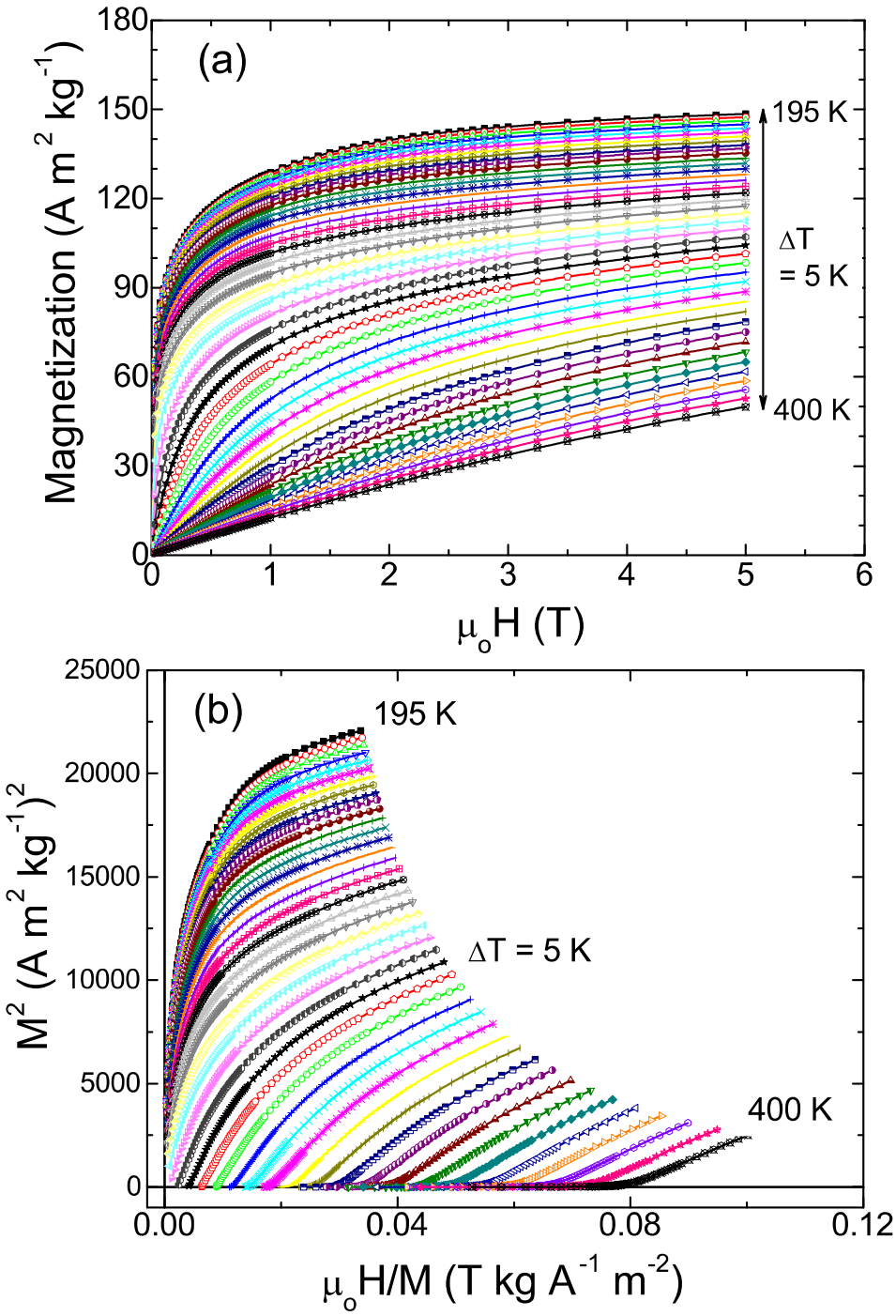
(a)
195 K
ΔT
= 5 K
400 K
Magnetization (A m$^2$ kg$^{-1}$)
$\mu_o$H (T)
(b)
195 K
ΔT = 5 K
400 K
M$^2$ (A m$^2$ kg$^{-1}$)$^2$
$\mu_o$H/M (T kg A$^{-1}$ m$^{-2}$)

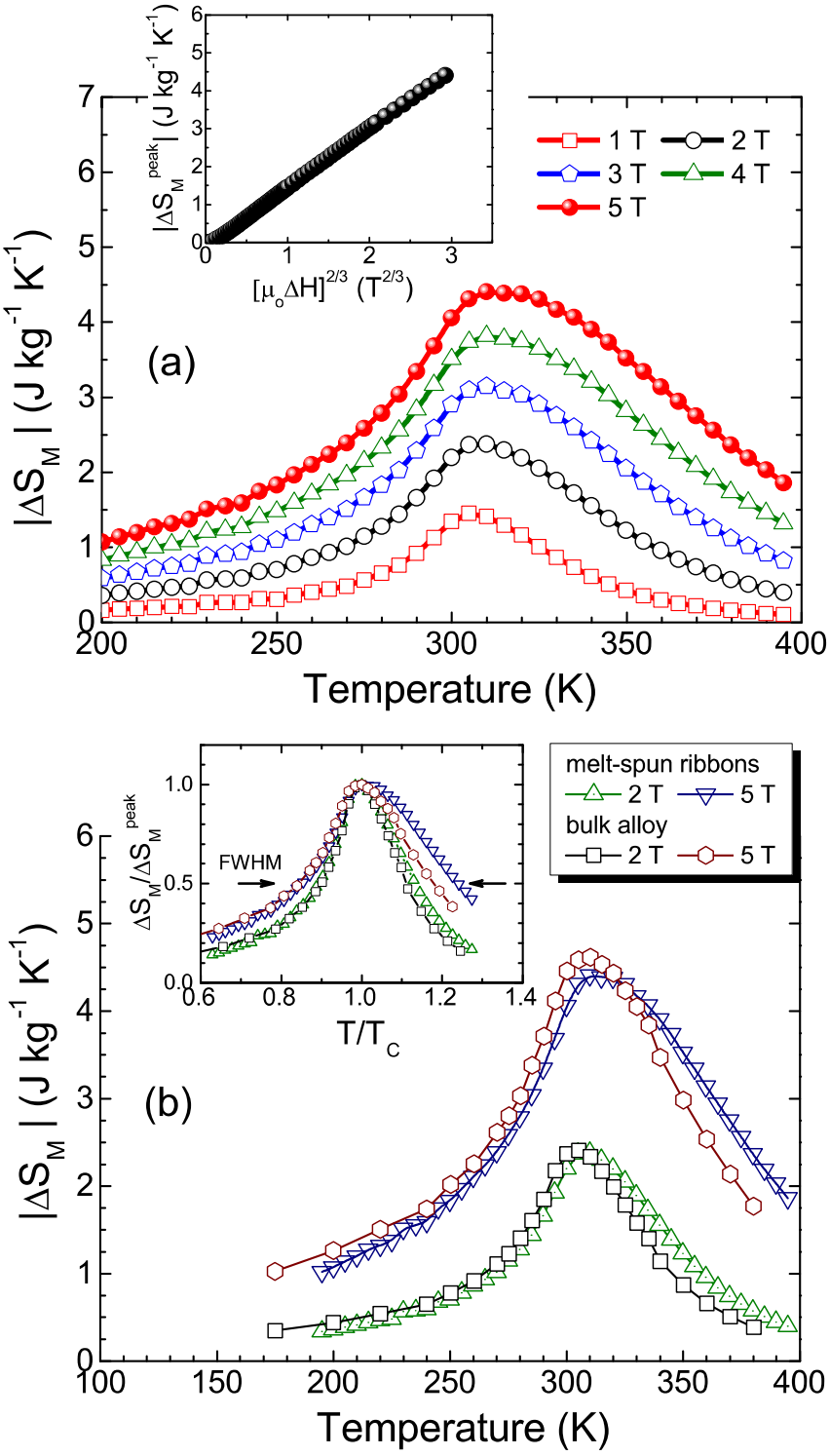
(a)
1 T
2 T
3 T
4 T
5 T
|ΔS_M| (J kg^-1 K^-1)
Temperature (K)
|ΔS_M^peak| (J kg^-1 K^-1)
[μ_oΔH]^2/3 (T^2/3)
(b)
melt-spun ribbons
2 T
5 T
bulk alloy
2 T
5 T
ΔS_M/ΔS_M^peak
FWHM
T/T_C

**FIGURE 5**

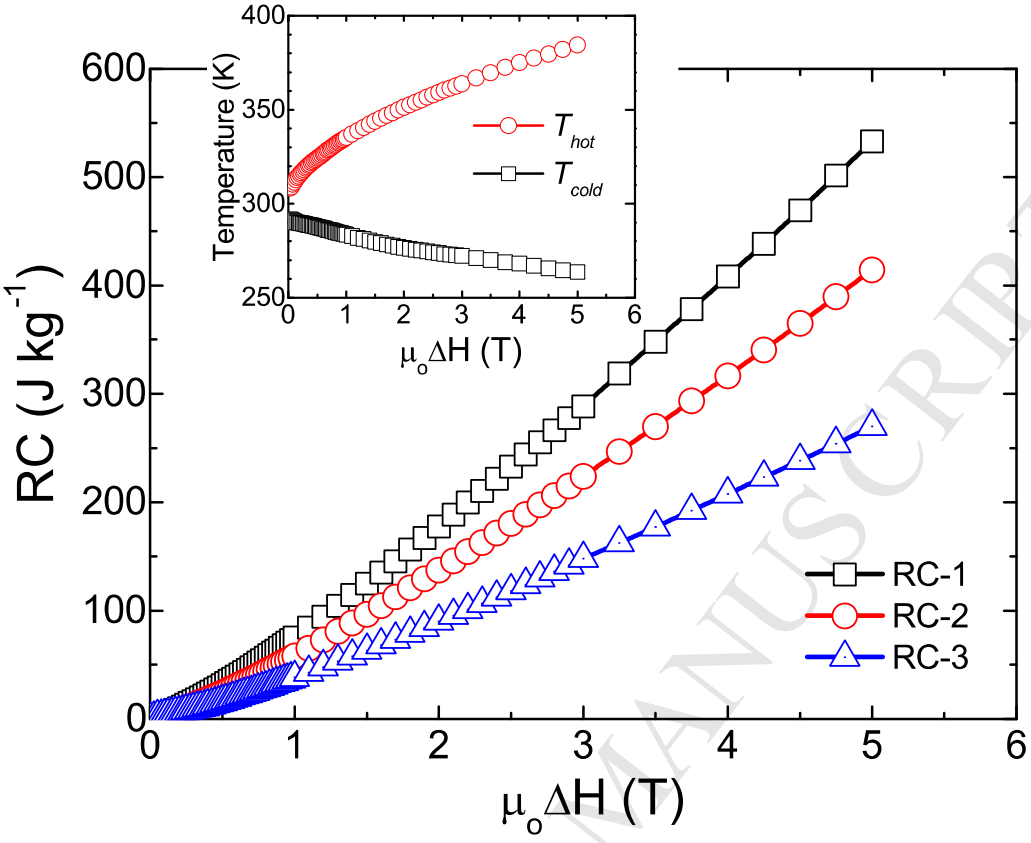


**FIGURE 6**

**Manuscript title:** "Investigating the magnetic entropy change in single-phase $Y_2Fe_{17}$ melt-spun ribbons":

**Authors:** J.L. Sánchez Llamazares, P. Álvarez-Alonso, C.F. Sánchez-Valdés, P.J. Ibarra-Gaytán, J. A. Blanco, and Pedro Gorria.

**Journal:** Current Applied Physics.

## Highlights

- Single-phase $Y_2Fe_{17}$ melt-spun ribbons obtained with hexagonal crystal structure.
- The one-step fabrication process circumvents any high-temperature annealing.
- We compare the magnetocaloric properties of the ribbons with those for bulk alloys.
- Both the refrigerant capacity and the working temperature range enhance about 15 %.